

Structural Basis of Prion Inhibition by Phenothiazine Compounds

Pravas Kumar Baral,¹ Mridula Swayampakula,¹ Manoj Kumar Rout,¹ Nat N.V. Kav,² Leo Spyropoulos,¹ Adriano Aguzzi,³ and Michael N.G. James^{1,*}

¹Department of Biochemistry, Faculty of Medicine and Dentistry, University of Alberta, Edmonton, AB T6G 2H7, Canada

²Department of Agricultural, Food and Nutritional Science, University of Alberta, Edmonton, AB T6G 2P5, Canada

³Department of Pathology, Institute of Neuropathology, University Hospital Zurich, Zurich 8091, Switzerland

*Correspondence: michael.james@ualberta.ca

<http://dx.doi.org/10.1016/j.str.2013.11.009>

SUMMARY

Conformational transitions of the cellular form of the prion protein, PrP^C, into an infectious isoform, PrP^{Sc}, are considered to be central events in the progression of fatal neurodegenerative diseases known as transmissible spongiform encephalopathies. Tricyclic phenothiazine compounds exhibit antiprion activity; however, the underlying molecular mechanism of PrP^{Sc} inhibition remains elusive. We report the molecular structures of two phenothiazine compounds, promazine and chlorpromazine bound to a binding pocket formed at the intersection of the structured and the unstructured domains of the mouse prion protein. Promazine binding induces structural rearrangement of the unstructured region proximal to β 1, through the formation of a “hydrophobic anchor.” We demonstrate that these molecules, promazine in particular, allosterically stabilize the misfolding initiator-motifs such as the C terminus of α 2, the α 2- α 3 loop, as well as the polymorphic β 2- α 2 loop. Hence, the stabilization effects of the phenothiazine derivatives on initiator-motifs induce a PrP^C isoform that potentially resists oligomerization.

INTRODUCTION

Transmissible spongiform encephalopathies (TSEs), also known as prion diseases, affect humans and a variety of mammalian species (Aguzzi and Polymenidou, 2004). These diseases are progressive, degenerative disorders of the CNS that result in dementia, significant motor dysfunction, and ultimately lead to death (Collinge, 2001). Human prion diseases exhibit highly heterogeneous clinical and pathological manifestations (Richardson and Masters, 1995). The sporadic Creutzfeldt-Jakob disease (CJD) is the most common form of prion disease in humans, affecting ~1–2 persons per million annually worldwide; CJD has symptoms of rapidly progressing dementia with a median survival of 4–6 months (Heinemann et al., 2007). Two less common human prion diseases are the acquired and the inherited forms; the acquired form develops in healthy humans after exposure to contagious agents, whereas genetic mutations

in the prion protein gene lead to inherited prion diseases presenting with various clinicopathological symptoms including classic CJD, Gerstmann-Straussler-Scheinker (GSS) disease, and fatal familial insomnia (FFI) (Prusiner, 2001).

The aggregation of a soluble protein into an insoluble, β sheet-rich amyloid fibril is a defining characteristic of many neurodegenerative diseases such as Alzheimer's, Parkinson's, and Huntington's diseases, including prion disorders (Brundin et al., 2010). Experimental evidence now suggests a unifying “prion-like” mechanism underlying these diseases; the misfolded protein aggregates induce a self-perpetuating process that leads to amplification and cell-to-cell spreading of the pathogenic protein assembly. A hallmark of prion disease is the accumulation of amyloid fibrils in brain tissue, resulting in excessive neuronal degeneration and spongiosis (Will, 1999). The conversion of ubiquitously present normal cellular prion protein (PrP^C) into a pathogenic conformation (PrP^{Sc}) is a crucial step for the onset of this disease. PrP^C is an extracellular membrane anchored protein that contains a flexible, unstructured N-terminal domain and a globular C-terminal domain comprising two short native antiparallel β strands, β 1 and β 2, and three α helices, α 1, α 2, and α 3. The pathogenic conformation PrP^{Sc} is polymeric, heterogeneous in terms of quaternary structure, and enriched in β sheets; PrP^{Sc} also possesses abnormal physicochemical properties such as protease resistance, insolubility, and the propensity to polymerize into amyloid-like fibrils. The transmission of TSE is essentially a PrP^{Sc}-dependent phenomenon; PrP^{Sc} acts as a template for self propagation by recruiting normal cellular PrP molecules in a cyclic fashion, leading to the formation of amyloid fibrils (Castilla et al., 2005; Sigurdson et al., 2009).

Currently, there are no therapeutic approaches to prevent or reverse the progressive and ultimately fatal course of human prion diseases. A handful of chemical chaperones from various molecular families, including polyanionic, tricyclic, tetrapyrrolic, polyene antibiotics, tetracycline, β sheet breaker peptides, Congo red, and others, have been found to have antiprion properties in cell culture models of prion disease (Bertsch et al., 2005; Kocisko et al., 2003). Measurement of PrP^{Sc} levels in infected neuroblastoma cell culture is an efficient protocol for qualitative and quantitative analysis of antiprion compounds (Solassol et al., 2003). However, the molecular targets and mechanisms of action for the active compounds remain unknown. Given the diverse group of chemical moieties that exhibit antiprion properties, it is plausible that their modes of action involve different

Table 1. Data Collection and Refinement Statistics

Complex	POM1Fab:moPrP: promazine	POM1Fab:moPrP: chlorpromazine
Data collection statistics	SSRL	APS
Space group	C2	C2
Resolution, Å	50.0–1.9 (1.97–1.90)	50.0–2.2 (2.28–2.20)
Completeness (%)	98.3 (85.1)	97.3 (86.4)
R_{merge}^a	0.09 (0.62)	0.08 (0.57)
I/σ	15.4 (2.0)	14.0 (1.5)
Redundancy	4.1 (3.2)	3.5 (2.2)
Total number of reflections	213,303	112,455
Unique reflections	52,155	32,491
Cell dimensions		
a, b, c (Å)	83.21, 106.03, 75.73	83.26, 106.88, 75.59
α, β, γ (°)	90, 95.68, 90	90, 95.32, 90
Refinement		
R_{work}^b	0.21	0.20
R_{free}^b	0.24	0.23
Total number of atoms	4,630	4,649
Protein	4,203	4,205
Ligand/Ions	20	21
Water molecules	407	423
Average B-factor (Å ²) ^a	41.33	51.37
Protein	41.29	51.37
Water molecules	45.81	61.21
Rmsd		
Bond lengths (Å)	0.005	0.008
Bond angles (°)	1.084	1.269

The data in parentheses refer to the reflections in the highest resolution shell.

^a $R_{\text{merge}} = \sum_{hkl} \sum_i |I_i(hkl) - \langle I(hkl) \rangle| / \sum_{hkl} \sum_i I_i(hkl)$, where $\langle I(hkl) \rangle$ is the mean intensity for multiply recorded reflections.

^b R_{work} and $R_{\text{free}} = \sum_{hkl} (|F_{\text{obs}}| - |F_{\text{calc}}|) / \sum_{hkl} |F_{\text{obs}}|$, for reflections in the working and test sets (5% of the data).

molecular targets or unrelated mechanisms. At the molecular level, rational design of small molecule therapeutics against prion disease can involve stabilization of PrP^C, clearance of PrP^{Sc}, or inhibition of the process of conversion between these prion protein isoforms. Stabilizing the native fold of PrP^C is likely the most prudent approach, as this may remove substrate from pathogenesis while preserving normal cellular function.

Among the diverse group of antiprion compounds, tricyclic molecules like promazine, chlorpromazine, acepromazine, and quinacrine appear to be promising candidates for immediate application in the treatment of prion diseases, as these compounds are currently used for the treatment of other ailments and have well-established safety profiles (Goodman and Gilman, 1970). In two independent studies, incubation of quinacrine induces clearance of protease-resistant PrP^{Sc}, after a persistent prion infection of neuroblastoma cells (Doh-Ura et al., 2000; Korth et al., 2001). However, in vivo administration of quinacrine in human clinical studies resulted in a mixed outcome. In some

patients, quinacrine treatment improved clinical symptoms transiently, whereas in others, beneficial effects were not observed (Nakajima et al., 2004). Thus, the positive in vitro effects of PrP^{Sc} inhibitors, as well as the potential efficacy from in vivo studies (Cronier et al., 2007) suggest that determining the molecular basis for their mechanism of action will aid in the design of therapeutic agents against prion and prion-like diseases.

In this study, we present the molecular crystal structure of the prion protein bound to two phenothiazine compounds, promazine and chlorpromazine. The role of these molecules in the stabilization of PrP^C was also analyzed using nuclear magnetic resonance (NMR) spectroscopy and molecular dynamics simulations. We show that these antiprion compounds bind to a well-defined hydrophobic pocket maintained by residues from helix α_2 and the antiparallel β strands, β_1 and β_2 . We suggest the binding of promazine could stabilize several PrP^C motifs that have previously been implicated in the transition of PrP^C to a neurotoxic state.

RESULTS

We have determined the molecular structures of promazine and chlorpromazine bound to the recombinant mouse prion protein (moPrP) by forming crystals of the ternary complexes of POM1 Fab:moPrP:promazine and POM1 Fab:moPrP:chlorpromazine; the structures were solved and refined by X-ray crystallographic methods to resolutions of 1.9 Å and 2.2 Å, respectively (Table 1). After several unsuccessful attempts to cocrystallize POM1 Fab:moPrP:compound, we relied on the soaking the POM1 Fab:moPrP crystals in solutions of the compounds. The POM1 Fab was used as a crystallization aid for the moPrP (117–230), given that crystallization of the moPrP alone is difficult with nonreproducible outcomes. Another advantage of using POM1 Fab to facilitate crystallization is that the binding interface is relatively small, leaving ~91% (~5,710 Å²) of the surface area of moPrP accessible for compound binding (Baral et al., 2012). The residue numbering scheme presented here for moPrP is in accordance with that of huPrP.

Phenothiazine Binding Site at the Intersection of β_1 - β_2 and α_2

Promazine is bound in a pocket formed by the side chains of residues on α_2 , β_2 , and β_1 that lie opposite to the binding epitope of POM1 Fab (Figure 1A). The tricyclic phenothiazine ring of the promazine is bent around bonds C1-N-C12 and C6-S-C7 giving the molecule a butterfly appearance having a dihedral angle of 135° between the aromatic planes (Figure 1A and Figure S1 available online). The dimethylaminopropyl side chain that is attached to the N-atom of the phenothiazine ring has an approximately “all staggered” conformation and extends above the convex side of ring. The phenothiazine part of promazine is bound in a predominantly hydrophobic pocket comprised of the residues Val122, Leu125, Tyr128, Tyr162, Ile182, Gln186, Val189, and Thr190, with the tricyclic scaffold stacked between the side chains of Leu125 on one side and Gln186 on the other (Figures 1B and 2A). The dimethylaminopropyl side chain protrudes outside the binding pocket while making hydrophobic contacts with the side chains of Val122 and Tyr162. The 2.2 Å crystal structure of POM1 Fab:moPrP:chlorpromazine displays

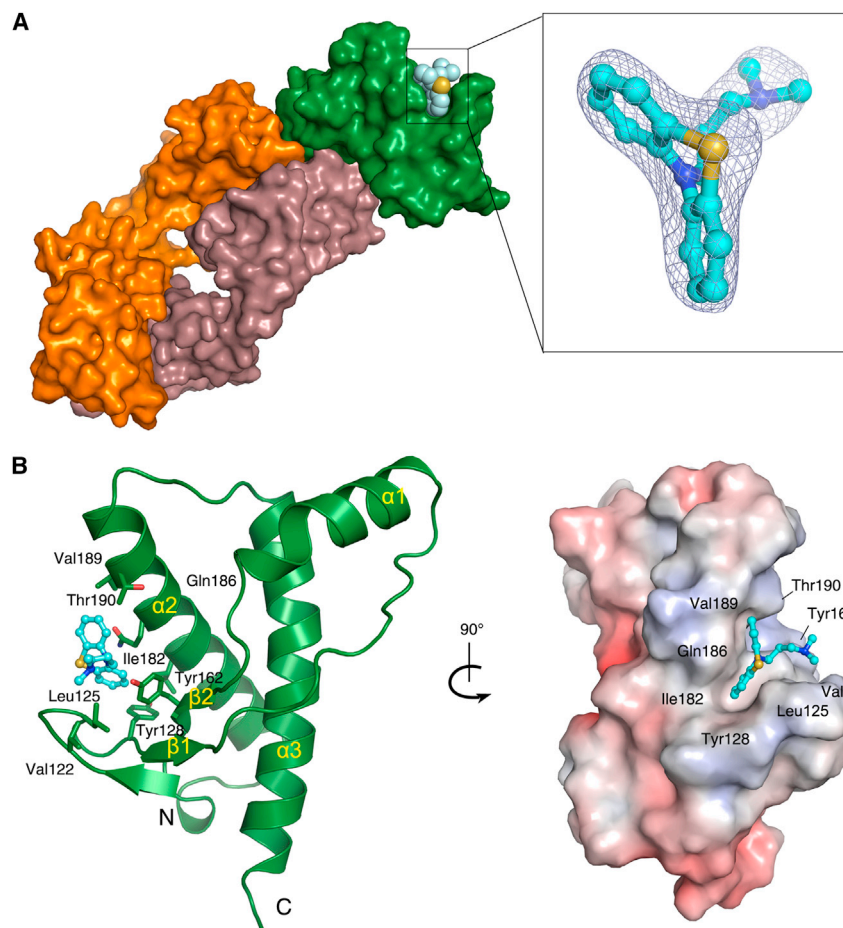


Figure 1. Crystal Structure of POM1 Fab:moPrP:promazine

(A) The complex of POM1 Fab:moPrP in the surface representation. POM1 Fab light chain, heavy chain, and mouse prion protein are colored orange, brown, and green, respectively. Promazine is shown in the space-filling representation with carbon, nitrogen, and sulfur atoms colored cyan, blue, and yellow, respectively. The electron density is contoured at 0.75σ from a $2|F_o| - |F_c|$ map, promazine is shown as in a ball and stick representation.

(B) moPrP residues in contact with promazine are shown as sticks, whereas promazine is shown as a ball and stick model. The electrostatic surface of moPrP is oriented to show the hydrophobic binding pocket, with promazine shown as a ball and stick model.

See also [Figure S1](#).

weak electron density for chlorpromazine, indicating that the bound chlorpromazine is only partially occupied ([Figure S2A](#)). Chlorpromazine contacts residues Leu125 and Gln186 of moPrP, these two residues bind promazine from opposite sides of the tricyclic ring. In the present interpretation, the mode of binding of chlorpromazine is different from that of promazine, although both molecules recognize a similar hydrophobic surface region on moPrP.

Structural superposition of the prion protein molecules in the free (Protein Data Bank [PDB] ID: 4H88) and ligand bound states have an overall root-mean-square deviation (rmsd) of 0.3 \AA for the $C\alpha$ atoms (residues 125–225), indicating that there are no significant structural changes in the folded prion domain upon compound binding. However, the side chains of the residues involved in the interaction with promazine show conformational changes that accommodate the hydrophobic ligand inside the binding pocket. In the bound structure, the side chain of Gln186 shifts by 108° at the C^β position, accommodating a hydrophobic contact with the convex face of the phenothiazine ring ([Figures 2A–2C](#)). The side chains of Tyr128 and Lys185 rearrange within the binding pocket and together contribute $\sim 60 \text{ \AA}^2$ to the interaction surface ([Figures 2A–2C](#)). For free moPrP, access to the binding site is restricted by the close side-chain packing of Leu125 and Lys185 that reside on opposite sides of the pocket; a gap of 5 \AA is observed between the ϵ -amino group

of Lys185 and the $C^{\delta 2}$ atom of the aliphatic side chain of Leu125 ([Figures 2B and 2C](#)). In the bound conformations, the C^α atoms of residues Gly124 and Leu125 show a shift of $\sim 4\text{--}5 \text{ \AA}$ that results in a movement of Leu125 away from Lys185, rendering the binding pocket more accessible ([Figures 2A–2C](#)). In the chlorpromazine bound structure, similar main-chain and side-chain positional shifts for Leu125 and Lys185 are observed, however, to positions that are intermediate between the conformations observed for the free and promazine

bound states ([Figure 2C](#)). The side chain of Gln186 exhibits a conformational change in the promazine bound structure, but not in the chlorpromazine bound state. We speculate that the structure of the chlorpromazine complex may represent an intermediate stage encountered while making its passage to the binding pocket ([Figure S2](#)).

Phenothiazine Binding Induces the Formation of a “Hydrophobic Anchor” at Residues 119–124 of the N-Terminal Region

The native prion protein has a structured domain comprising three helices ($\alpha 1$, $\alpha 2$, and $\alpha 3$), two short antiparallel β strands ($\beta 1$ and $\beta 2$), and a long, disordered N-terminal domain from residues 23–124. The electron density for residues 119–124 becomes defined upon promazine binding ([Figures 2D and S3](#)). This leads to a structural rearrangement at the N terminus of the structured domain of moPrP (residues 117–124), through the formation of an additional β strand that is antiparallel to $\beta 1$; this strand was previously shown to be flexible in the moPrP NMR structures ([Figure S3](#)). These changes occur in the vicinity of a second POM1 Fab:moPrP complex molecule; the proximity of POM1 Fab possibly explains why the attempts at cocrystallization with phenothiazine compounds were not successful ([Figures S2C and S2D](#)). In the unbound POM1 Fab:moPrP crystal structure, there is a narrow gap present around the $\beta 1$ – $\beta 2$ region,

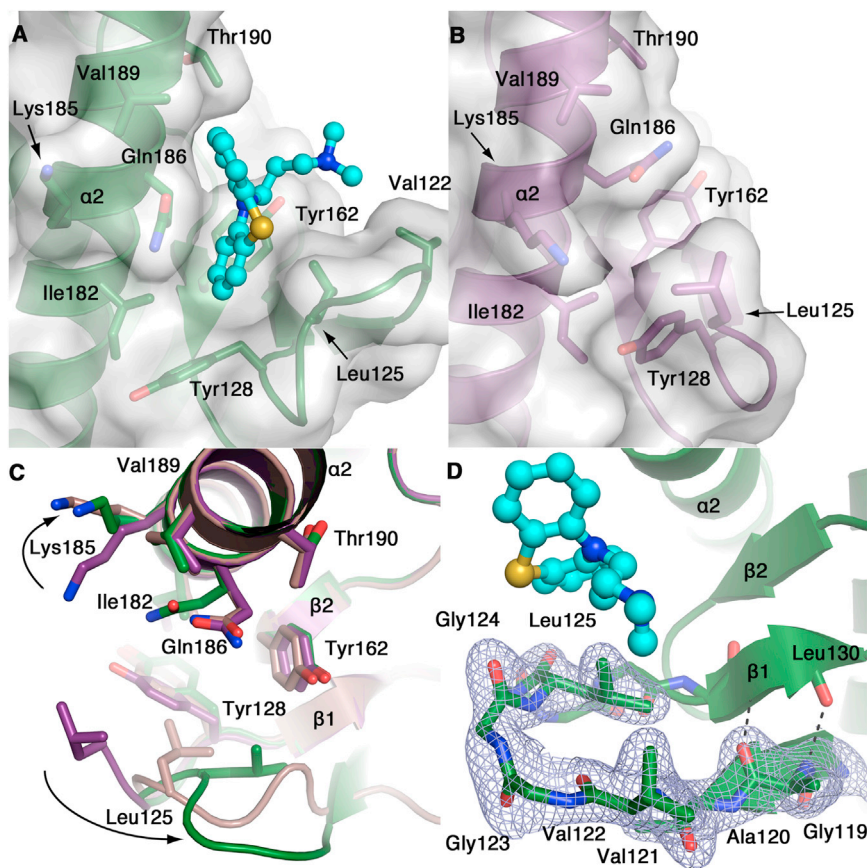


Figure 2. Structural Changes upon Binding of Phenothiazine Derivatives

(A) Surface representation of moPrP (green) bound to promazine with interacting residues shown as sticks and promazine shown as a ball and stick model with the carbon, nitrogen, and sulfur atoms colored cyan, blue, and yellow, respectively.

(B) Surface representation of moPrP in the free conformation (PDB ID: 4H88, violet).

(C) Superposition of bound and free moPrP structures: moPrP:promazine in green, moPrP: chlorpromazine in gray, and free moPrP in violet. Residues in contact with the phenothiazine derivatives are shown as sticks. Conformational changes induced by phenothiazine binding are indicated by arrows.

(D) The $2|F_o| - |F_c|$ electron density map for residues 119–128 is shown at 1σ with moPrP residues (green) shown as sticks.

See also Figure S2.

between the two neighboring protein complexes and with no contacts between the molecules. However, upon promazine binding the additional beta strand is formed in this gap region while making contacts with the adjacent protein complex. There is only room for a few amino acids to be accommodated in this region and therefore, the His-tag cleaved moPrP (120–230) and moPrP (117–230) constructs produced the electron density for the ligand as well as for the disordered moPrP region prior to residue Leu125. However, in the absence of the compound, this beta strand is not observed indicating that the formation of the beta strand in the unstructured moPrP region (residues 117–124) is dependent on the compound binding. In this antiparallel β -arrangement, however, the previously unstructured N-terminal region forms backbone hydrogen-bonded interactions with strand β 1; the main-chain amide and the carbonyl group of Ala120 form hydrogen bonds with the main-chain carbonyl and the amide group of Leu130, respectively (Figure 2D). Additionally, two tandem β -turns are observed in the unstructured region of residues 119–124 upon promazine binding; a type I β -turn is present between Val122–Leu125 and a type II β -turn is present between Leu125–Tyr128 (Figure S3). However, in the chlorpromazine bound structure, although the electron density for residues 119–124 is traceable, it is incomplete, hindering the structural interpretation for this region.

The side chains from residues Tyr128–Met129–Leu130 (YML) of strand β 1 and Tyr162–Tyr163–Arg164 (YYR) of β 2 are closely packed together through systematic interstrand hydrophobic

pairing (Tyr128:Arg164, Met129:Tyr163, and Leu130:Tyr162) both above and below the plane of the short, antiparallel β sheet (Figure 3B). In the presence of promazine, we observe analogous hydrophobic interactions, in the unstructured region adjacent to the YML and YYR motifs; the side chains of the residues belonging to the unstructured N terminus, 119 GAVVGGGL 125 , and residues from the β 1– β 2 region are engaged in hydrophobic interactions (Figure 3A). The side chain of Leu125 is packed against the side chain of Val122 from the β strand formed in the bound state, thus creating a “hydrophobic anchor” at this region. In addition, the side chain of Val122 interacts with the methyl group of the dimethylaminopropyl side chain of promazine. On the other side of the hydrophobic anchor, Leu125 is involved in hydrophobic interactions with the aromatic side chains of Tyr128 and Tyr162 located within 4–5 Å (Figure 3A). Similarly, below the plane of the β sheet, the side chains of Val121 and Met129 are within 4 Å, forming hydrophobic contacts. The formation of β sheet secondary structure in presence of phenothiazine-like compounds is likely an essential characteristic for the mechanism of PrP^{Sc} inhibition, as the hydrophobic dimethylaminopropyl side chain induces the formation of a well-defined structure within a disordered region of the prion protein. Previous structure activity relationship studies on tricyclic acridine and phenothiazine compounds indicate that the presence of long side chains attached to the central tricyclic scaffold is a vital requirement for inhibition; the absence of this feature, as in case of phenazine, phenothiazine, and 2-chlorophenothiazine, results in abolition of therapeutic benefit (Korth et al., 2001). The physicochemical nature of the side chain including length, flexibility, and hydrophobicity are essential parameters that can influence therapeutic outcomes, as rigid bonds at the tricyclic N-atom are known to reduce therapeutic efficacy significantly. The long, flexible, and hydrophobic side chain covalently attached to the acridine nitrogen of quinacrine is effective for

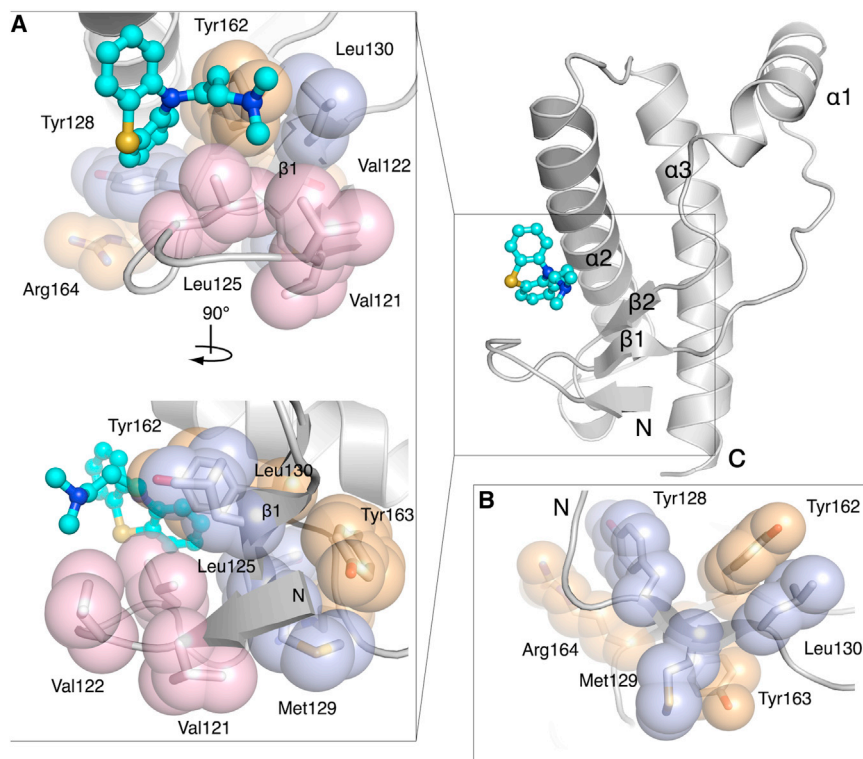


Figure 3. Formation of the Hydrophobic Anchor at the N Terminus

(A) Hydrophobic surface of Val121, Val122, and Leu125 shown in a space-filling models (pink) contact residues from strand $\beta 1$ (Tyr128, Met129, and Leu130, space-filling model, blue) and strand $\beta 2$ (Tyr162, Tyr163, and Arg164 space-filling model, orange).

(B) Hydrophobic interactions between residues from strands $\beta 1$ and $\beta 2$ are shown as space-filling models in blue and orange, respectively. Hydrophobic pairs Tyr128:Arg164 and Leu130:Tyr162 are formed above the β -plane, whereas Met129:Tyr163 is formed below the plane.

See also [Figure S3](#).

stabilizing secondary structure within regions that are otherwise disordered in the free state, whereas the tricyclic scaffold is bound to the structured prion domain.

Phenothiazine Binding Stabilizes the $\beta 2$ - $\alpha 2$ loop through a Hydrogen Bond Network

The residues within the $\beta 2$ - $\alpha 2$ loop are within ~ 10 Å from the binding pocket for phenothiazine compounds. Experimental evidence implicates this loop region in initiating PrP^{Sc} conversion and possibly influencing interspecies scrapie transmission (Damberger et al., 2011; Sigurdson et al., 2011). We observe that on binding to promazine, the side chain of Tyr128 from strand $\beta 1$ shows an inward movement of $\sim 45^\circ$ (at Chi-2), and Tyr128 forms a hydrogen bond between the hydroxyl group and a carboxylate oxygen of Asp178, present in helix $\alpha 2$ (Figure 4A). This inward shift of Tyr128 makes the aromatic side chain move ~ 3 Å closer toward Ile182 in helix $\alpha 2$ thereby increasing the hydrophobic contact surface. The native moPrP NMR structures show multiple orientations for the $\beta 2$ - $\alpha 2$ loop, under different experimental conditions (Figures 4C–4F). However, the additional interactions between the residues of strand $\beta 1$ and helix $\alpha 2$ in the presence of promazine influence the orientation of the $\beta 2$ - $\alpha 2$ loop. Various structures of moPrP in the free and bound states indicate that Tyr169 in the $\beta 2$ - $\alpha 2$ loop adopts several different conformational positions, ranging from an outward-facing solvent accessible orientation to an inward-facing, fully buried position, with additional orientations intermediate between open and buried (Figures 4A–4F), with concomitant backbone isoforms within this flexible region are also seen. The relative positions for the polar residues Arg164, Asp167, and Gln168 in the $\beta 2$ - $\alpha 2$ loop also change depending on the

loop backbone conformation. In the promazine bound structure, a cation- π interaction is observed between the side chains of Arg164 and Tyr128 residues; they are separated by 4 Å apart (Figure 4A). These side chain orientations appear to be an essential feature that could provide a stabilizing effect on the $\beta 1$ - $\beta 2$ sheet as well as on the $\beta 2$ - $\alpha 2$ loop region. However, in the absence of ligand, Arg164 and Tyr128 are separated by 4.8 Å, disrupting the potentially stabilizing cation- π interaction between these side chains (Figure 4B). Additionally, in the bound state, the hydrogen bonding interaction between Tyr128 and Asp178 stabilizes a side chain conformation of Asp178 that is suitable for Tyr169 to make a hydrogen bonding interaction with the carboxylate oxygen of Asp178 (Figure 4A). For the promazine bound structure, there are two hydrogen bonding interactions for Asp178, these involve Tyr128 and Tyr169. In the unbound moPrP structures, either a single or no hydrogen bond is observed (Figures 4B–4F). Although the bound and free states exhibit identical $\beta 2$ - $\alpha 2$ loop conformations, the bound state of the $\beta 2$ - $\alpha 2$ loop appears more stable and has additional interactions with Tyr128 that most likely prevent an easy transitioning of the Tyr169 side chain conformation.

Phenothiazine Binding Stabilizes the $\alpha 2$ - $\alpha 3$ Hydrophobic Core through Allosteric Interactions

The binding of promazine to ^{15}N -labeled shPrP(90–232) in solution was investigated using heteronuclear NMR spectroscopy. Chemical shift changes for the main chain amides of PrP upon titration of promazine to shPrP(90–232), were analyzed (Figures 5A and S4A). Most of the residues displaying significant chemical shift changes on binding to promazine were found to cluster into two separate regions of the prion protein. The first region is the $\alpha 2$ - $\alpha 3$ loop and the neighboring residues in helices $\alpha 2$ and $\alpha 3$. The second region is helix $\alpha 1$, specifically those residues in contact with $\alpha 3$. Among these two clusters, helix $\alpha 2$ is nearest to the promazine binding site, and Thr188 within $\alpha 2$ shows the largest chemical shift deviation upon promazine binding. Residues neighboring Thr188 such as Phe198 in the $\alpha 2$ - $\alpha 3$ loop, and Val203, Met206, and Val210 in helix $\alpha 3$ also show chemical

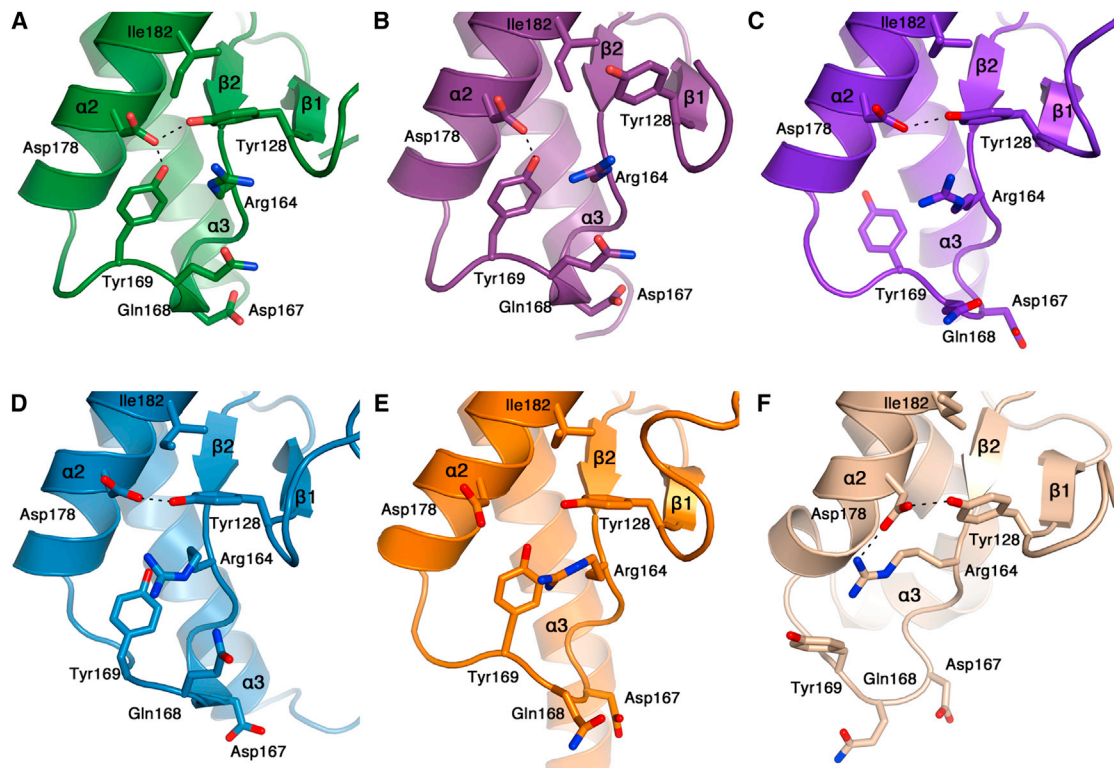


Figure 4. Conformational Heterogeneity at $\beta 2$ - $\alpha 2$ Loop Region

Side chains of selected residues are represented as sticks, with hydrogen bonds shown as dashed lines.

(A) In the moPrP:promazine crystal structure (green), Tyr128, Asp178, and Tyr169 form a hydrogen bonded network.

(B) In the moPrP crystal structure (PDB ID: 4H88, violet), Tyr128 lacks a hydrogen bond to Asp178.

(C) In the moPrP NMR structure (PDB ID: 1XYX, purple), Tyr128 is hydrogen bonded to Asp178, and Tyr169 is fully buried.

(D) In the moPrP NMR structure (PDB ID: 2L39, blue) Tyr128 is hydrogen bonded with Asp178, Tyr169 is partially buried, with an altered loop conformation.

(E) In the moPrP NMR structure (PDB ID: 2L1H, orange) there are no hydrogen bonding interactions between Tyr128, Tyr169, and Asp178.

(F) In the moPrP NMR structure (PDB ID: 1AG2, wheat), hydrogen bonds are present between Tyr128:Asp178 and Asp178:Arg164, and Tyr169 is completely surface-exposed.

shifts changes for the backbone amides (Figure S5B). As the residues of the $\alpha 2$ - $\alpha 3$ loop and the $\alpha 3$ helix are in contact with those of helix $\alpha 1$, small chemical shift changes are observed for some residues in $\alpha 1$. Thus, chemical shift changes are in agreement with the crystallographically determined structures for the promazine bound state. Addition of promazine to 12 mM (Figure S4A) produces a pattern of chemical shift changes similar to the addition of 6 mM, however, further increasing promazine concentration leads to protein aggregation. We observed linear changes in the chemical shifts upon addition of promazine that seems to indicate weak binding with shPrP. Furthermore, we observe chemical shift perturbations for residues distal from the promazine binding site; these changes reflect subtle structural changes that are transmitted through the various secondary elements of PrP upon ligand binding. Formation of the additional beta strand at the N-terminal region as seen in the crystal structure of POM1 Fab:moPrP:promazine could not be confirmed by NMR spectroscopy due to the lack of backbone resonance assignment for the residues 119–124 in shPrP. However, it is noteworthy that despite the use of two different systems—moPrP with POM1 Fab in X-ray crystallography and shPrP without POM1 Fab in NMR spectroscopy—

we obtained similar promazine binding results. Hence, we conclude that the promazine binding to the moPrP in the crystal structure of POM1 Fab:moPrP:promazine is not influenced by POM1 Fab binding.

Promazine Binding Attenuates PrP Flexibility

To assess the role of changes in protein dynamics upon drug binding, we conducted molecular dynamic (MD) simulations using the structured domain from moPrP (residues 119–225) in the presence and in the absence of promazine. Free moPrP shows flexibility within the $\alpha 2$ - $\alpha 3$ loop and the adjoining residues in helices $\alpha 2$ and $\alpha 3$ (Figure 6B). Per residue root-mean-square fluctuation (rmsf) values indicate a flexible region within the C-terminal half of the domain, near the end of helix $\alpha 2$ (190 TTTTK 194). Large amplitude B-factors for atoms from the C terminus of helix $\alpha 2$ and the $\alpha 2$ - $\alpha 3$ loop in various PrP X-ray structures (Figure S5A), and the different conformations observed in the NMR structural ensembles (Figure S3A), are consistent with the flexibility of these regions observed in the MD simulation. The C-terminal unwinding of the $\alpha 2$ helix may result from the consecutive Thr residues involvement in polar interactions with main-chain atoms of the $\alpha 2$ - $\alpha 3$ loop. The loss

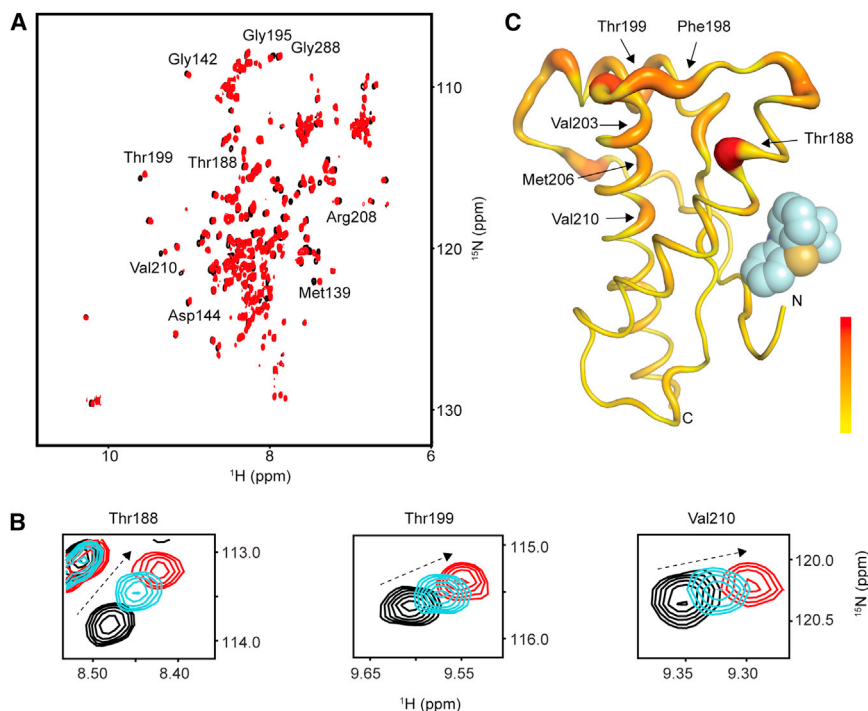


Figure 5. Stabilization of the Hydrophobic Core through Allosteric Interactions

(A) Overlay of the 2D ¹H-¹⁵N HSQC NMR spectra of shPrP90–232 in the absence (black) and presence of 6 mM (cyan) and 12 mM (red) promazine. (B) The inset shows individual residues having significant chemical shifts changes.

(C) The heat map showing residues from shPrP for which backbone amide resonances are attenuated by the addition of promazine, with red broad ribbons indicating maximum perturbation. See also Figure S4.

Promazine and chlorpromazine binding to prion protein induced the formation of a hydrophobic anchor between the N-terminal segment comprising Gly119–Gly124 and residues from β1 (Figure 3A and Table 2). The unstructured N-terminal part of the prion protein adjacent to the structured domain is responsible for prion toxicity; specifically, residues 106–126 from the mammalian prion protein (Ettaiche et al., 2000; Forloni et al., 1993).

This segment has been extensively studied both as a neurotoxic amyloid prion and as a potential mediator for the conversion of PrP^C to the scrapie form (Forloni et al., 1993; Jobling et al., 1999; Salmona et al., 1999; Selvaggini et al., 1993). The conserved palindromic sequence ¹¹³AGAAAAGA¹²⁰ within residues 106–126 has been implicated in the assembly of amyloid fibrils and neurotoxicity (Jobling et al., 1999; Lee et al., 2008). Solid state NMR structural data for PrP^C 106–126 peptide fibrils suggest the formation of a class-1 steric zipper motif constituting Gly114–Gly123, is involved in an extensive, interdigitated interface between two parallel beta sheets (Walsh et al., 2009). Given that this flexible, unstructured region of PrP^C exhibits a tendency to self-aggregate, binding of small molecules to this region may reduce the flexibility and facilitate formation of secondary structure, thereby providing a potential path to therapeutic intervention. Interestingly, the secondary structure induced by promazine and chlorpromazine binding results in the burial of Met129 from strand β1. This residue has been implicated in conformational selection of prion strains and confers susceptibility to prion diseases through the common human methionine-valine polymorphism at *PRPN* codon 129 (Collinge et al., 1996; Lewis et al., 2006; Wadsworth et al., 2004). Although Met129 polymorphism does not involve altering the native structure or the global stability of PrP (Hosszu et al., 2004), structural data on prion proteins suggest that an intermolecular four-stranded sheet formation from two adjacent prion protein molecules at strand β1 is possibly a crucial event in the transition to PrP^{Sc} (Figure S6) (Antonyuk et al., 2009; Lee et al., 2010). Sawaya et al. (2007) experimentally demonstrated that the formation and propagation of cross-β amyloid spines are essentially reliant on the primary stacking event of antiparallel beta strands, as observed in the PrP structures. Phenothiazine-induced formation of additional secondary structural elements may deter PrP stacking at

DISCUSSION

of helical structure at the C terminus of α2 perturbs the hydrophobic core network maintained by side chain interactions at the interface of the α2-α3 hairpin structure (Figures 6D, S5C, and S5D). Upon promazine binding, there is a significant reduction in the rmsf of the residues proximal to the binding site, for which Thr190 is involved in key interactions with promazine. During the time course of the simulation, the tricyclic compound was found to contact Ile182, Lys185, Gln186, and Val189 in α2. Interestingly, the secondary structure over the course of the simulation (Figures 6A, S5C, and S5D), indicates that the helical content of α2 remains stable on binding promazine, likely as a result of close hydrophobic interactions between the promazine and moPrP. Recent long timescale simulations (1 μs) for ovPrP (sheep prion) indicate that loss of the C-terminal helical structure for helix α2 is a critical step in the conversion of PrP^C into the β-rich conformer (Chakroun et al., 2013).

Despite tremendous progress in the field of prion biology, the molecular events responsible for PrP^{Sc} formation from cellular prion protein remain elusive. There is general consensus regarding the posttranslational, multistep refolding processes, in which the native PrP^C undergoes the malicious conformational changes leading to the assembly of β sheet-rich, protease-resistant PrP^{Sc} molecular aggregates. Once formed, PrP^{Sc} recruits partially folded, nonnative intermediates, a process that leads to formation of long fibrillar structures, as observed through many biophysical techniques (Caughy et al., 2009). Although there is ample evidence suggesting the existence of aberrant prion intermediates, the precise involvement for the various secondary structural elements of PrP^C in amyloid formation is unknown.

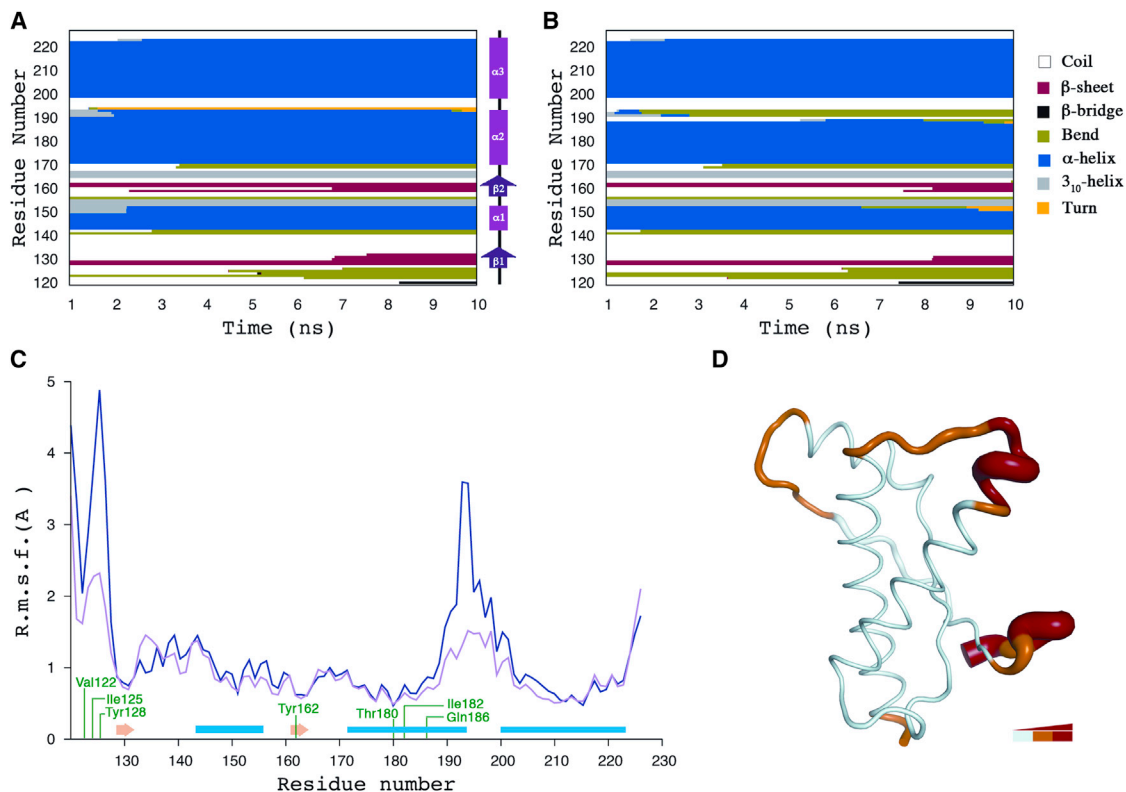


Figure 6. Promazine Acts as an Attenuator of Flexibility

(A and B) Time-dependence for the secondary structure of moPrP (A), in the presence and (B), in the absence of promazine during MD simulations, respectively. (C) Rmsf for the moPrP protein during MD simulations in the presence (pink) and in the absence of promazine (blue). Alpha helices and β strands are shown in blue and yellow, respectively, promazine binding residues are indicated by green lines.

(D) Ribbon representation for the backbone atoms of moPrP in the unbound state, backbone rmsf values are represented by the width of the ribbon and colored according to the magnitude of atomic fluctuations.

See also [Figure S5](#).

strand $\beta 1$, particularly in the vicinity of Met129, and arrest the toxic consequences of oligomer formation.

It has been suggested that PrP subdomains $\beta 1$ - $\alpha 1$ - $\beta 2$ and $\alpha 2$ - $\alpha 3$ must be separated in order to promote PrP^{Sc} formation, as chemical tethering of these subdomains through the introduction of disulfide bridges prevents toxic conversion ([Hafner-Bratkovic et al., 2011](#)). In the promazine bound structure of moPrP, we observe an analogous tethering of these subdomains; the $\beta 1$ - $\alpha 1$ - $\beta 2$ motif, with the help of the hydrophobic anchor prior to strand $\beta 1$, attaches strongly to helix $\alpha 2$, with the hydrophobic tricyclic phenothiazine scaffold present at the interface ([Figure 3A](#)). In addition, the binding of promazine leads to burial of the YYR motif in strand $\beta 2$; this motif was previously shown to be preferentially exposed in PrP^{Sc}, in the denatured form of PrP^C, but not in the cellular isoform, PrP^C ([Paramithiotis et al., 2003](#)). Furthermore, it has been demonstrated that a primary step in the urea induced denaturation of PrP^C involves unfolding of the native β sheet ([Julien et al., 2009](#)). The phenothiazine molecules bound to PrP^C provide additional stability to this β sheet region as they bind to PrP^C at a critical site, where residues from both strands $\beta 1$ and $\beta 2$ are able to contact the tricyclic ring.

Recently, the $\beta 2$ - $\alpha 2$ loop region of the prion protein has attracted intense interest with respect to its potential role in

the onset of TSEs ([Christen et al., 2013](#)). Specific residues in this labile region, between positions 167 and 170 have been shown to increase susceptibility to interspecies prion transmission, as well as leading to spontaneous PrP^{Sc} generation in transgenic mice ([Agrimi et al., 2008](#)). Structural studies indicate surface polymorphism of this region due to the “in” and “out” conformational transitioning of residue Tyr169 ([Christen et al., 2013](#)). The solvent-exposed out conformation leads to increased hydrophobicity in the loop structure and has been linked to cytotoxicity ([Corsaro et al., 2011](#)). The $\beta 2$ - $\alpha 2$ loop has two known distinct backbone conformations, a 3_{10} -helix, seen in the majority of the PrP^C structures, and an aberrant type-I β -turn structure, seen in a few PrP^C conformations, that may increase the propensity for transitioning to PrP^{Sc}. In both the bound and unbound forms of moPrP structures, the $\beta 2$ - $\alpha 2$ loop acquires a 3_{10} -helix conformation with Tyr169 having an in conformation. However, in the presence of promazine, an additional hydrogen bond network is formed between residues Tyr128, Tyr169, and Asp178, that stabilizes the $\beta 2$ - $\alpha 2$ loop. On this basis, we propose that the Asp178 to Asn mutation, as found in FFI, destabilizes the $\beta 2$ - $\alpha 2$ loop giving rise to a type-I β -turn conformation due to disruption of the hydrogen bond network.

Table 2. Backbone ϕ and ψ Torsion Angles Measured for the N Terminus Region, Residues 119–129 of moPrP

Residue Number	Amino Acids	Φ ($^\circ$)	Ψ ($^\circ$)
119	GLY	—	151.1
120	ALA	−100.0	140.2
121	VAL	−114.9	136.0
122	VAL	−140.1	−170.9
123	GLY	9.3	−112.4
124	GLY	−124.2	79.0
125	LEU	−92.2	−4.3
126	GLY	54.4	48.2
127	GLY	95.7	−21.8
128	TYR	−79.4	156.8
129	MET	−129.5	153.6

Several mutations in the structured domain of prion protein that have been implicated in the conversion to the scrapie form significantly affect the thermodynamics and stability of PrP^{Sc} (van der Kamp and Daggett, 2010). An extensive hydrophobic network between helical secondary structures in the folded domain forms the hydrophobic core of the prion protein. The pathogenic mutations V180I (CJD), F198S (GSS), V203I (CJD), and V210I (CJD), are found at the interface of helices $\alpha 2$ and $\alpha 3$ (Figure S5B); these mutations significantly alter the dynamic equilibrium between folded and unfolded states of the hydrophobic core, leading to the PrP^{Sc} formation (Apetri et al., 2004). Molecular dynamics simulations for ten disease-associated mutations in PrP show significant structural perturbations at the $\alpha 2$ - $\alpha 3$ hairpin interface, the major component of the hydrophobic core (Meli et al., 2011). Our NMR chemical shift data indicate that promazine binding perturbs the interface between helices $\alpha 2$ - $\alpha 3$, supporting the idea that promazine binding may allosterically enhance the packing between the helices. Consistent with the NMR experiments, the molecular dynamics simulations we conducted show that promazine binding attenuates the flexibility of the C-terminal region of helix $\alpha 2$, thereby facilitating more extensive interhelical packing. This flexible prion region, the C-terminal part of helix $\alpha 2$ and the $\alpha 2$ - $\alpha 3$ loop, is the recognition site for antiprion compound GN8, a small molecule that prolongs the survival of TSE-infected mice (Kuwata et al., 2007). The promazine binding site is adjacent to that of GN8, and the overlapping epitope regions for these molecules on the prion protein share Val189, a residue which forms part of the C terminus of helix $\alpha 2$.

We have demonstrated that phenothiazine derivatives facilitate the prevention of PrP misfolding through a multifaceted protein stabilization mechanism. Promazine elicits a chaperone-like effect at three noncontiguous toxic motifs of the PrP^C molecule: the antiparallel $\beta 1$ - $\beta 2$ region, $\beta 2$ - $\alpha 2$ loop, and the C-terminal part of helix $\alpha 2$. In addition to the stabilizing effect on various PrP^C motifs, burial of both the aggregation prone N-terminal flexible region and Met129 are essential to the stabilization mechanism of this antiprion compound. Formation of the scrapie form of the prion protein from cellular PrP may involve concerted structural perturbations in different motifs of the folded domain, coupled to preferential exposure of the aggrega-

tion prone prion region, which subsequently interacts with contagious agents. This is evident from the diverse natures of the extrinsic and intrinsic factors that are responsible for initiating the pathological conversion process of prion protein to the scrapie form. A key step in the conversion likely involves prion misfolding, initiated by individual toxic motifs separately or in combination (Figure 7). These intermediate states for PrP^C have been recognized to lead to aberrant self-assembly.

Our structural data for small-molecule binding to the prion protein uncovers the phenothiazine recognition site on the prion protein and illuminates the allosteric mechanism by which stability is imparted to misfolding-prone regions. The antimalarial, tricyclic acridine derivative quinacrine, failed to produce a favorable outcome in clinical trials involving CJD patients (Collinge et al., 2009; Geschwind et al., 2013), despite promising results in cell-culture models (Korth et al., 2001). This discrepancy between in vitro and in vivo studies, whether related to pharmacokinetic and/or pharmacodynamic properties of quinacrine, is a matter of further investigation. However, the emergence of a drug resistant strain of PrP^{Sc} due to the continuous treatment of PrP diseases with quinacrine (Ghaemmaghami et al., 2009) perhaps indicates a shifting of the misfolding center to other motifs that are not stabilized by quinacrine. This behavior of the prion protein supports the idea of a multi-focal nature for the initiation of misfolding. In this scenario, we propose that multiple antiprion drugs with unrelated molecular mechanisms of action may be administered in a simultaneous fashion to elicit a cumulative and more beneficial effect. Our high-resolution structural data will be very useful toward enhancing the therapeutic potential of tricyclic compounds through a structure-guided approach.

EXPERIMENTAL PROCEDURES

Cloning, Expression, and Purification of moPrP(117–230)

The expression vector pET15b (Novagen) was used for the expression of the mouse PrP(117–230). For cloning, two primers flanking the PrP117–230 region of the full-length mouse Prion protein were designed with the BamH1 and EcoR1 restriction sites, respectively. Upon PCR amplification, this insert was incorporated into the multiple cloning site of pET15b vector between the BamH1 and EcoR1 restriction sites. The fidelity of the cloned gene was validated by sequencing. Upon confirming the sequence, the plasmid was transformed into BL21-CodonPlus (DE3)-RIL cells (Stratagene) by heat-shock. The cells were grown in Luria-Bertani (LB) broth containing 0.1 mg/ml ampicillin and 0.34 mg/ml chloramphenicol at 37°C, 200 rpm, and the PrP(117–230) expression was induced in the inclusion bodies using 0.1 M isopropyl β -D-1-thiogalactopyranoside (IPTG). The inclusion bodies were sonicated, pelleted by centrifugation, and extensively washed. Subsequently, the inclusion bodies were incubated in a denaturing buffer G of 8 M Urea, 10 mM Tris-HCl, 100 mM NaH₂PO₄, and 5 mM reduced glutathione pH 8.0 for 1 hr at room temperature with constant stirring. The extracted denatured PrP(117–230) was purified using metal affinity chromatography by loading onto a Ni-NTA agarose column (QIAGEN). The bound PrP(117–231) was refolded on-column by gradient application of buffer G (denaturing buffer) to buffer A (10 mM Tris-HCl, 100 mM NaH₂PO₄, 5 mM imidazole, pH 8.0) as described by Yin et al. (2003). After the refolding, the nonspecifically bound impurities were removed by washing with 10 mM Tris-HCl, 100 mM NaH₂PO₄, 50 mM imidazole, pH 8.0. Finally, the pure PrP(117–230) was eluted with the elution buffer containing 10 mM Tris-HCl, 100 mM NaH₂PO₄, 400 mM imidazole pH 5.8. The obtained protein was exchanged into distilled water using Amicon Ultra centrifugal filters (3 kDa molecular weight cutoff; Millipore). The purity was confirmed by SDS-PAGE and the concentration was determined by the Bradford method (Bradford, 1976).

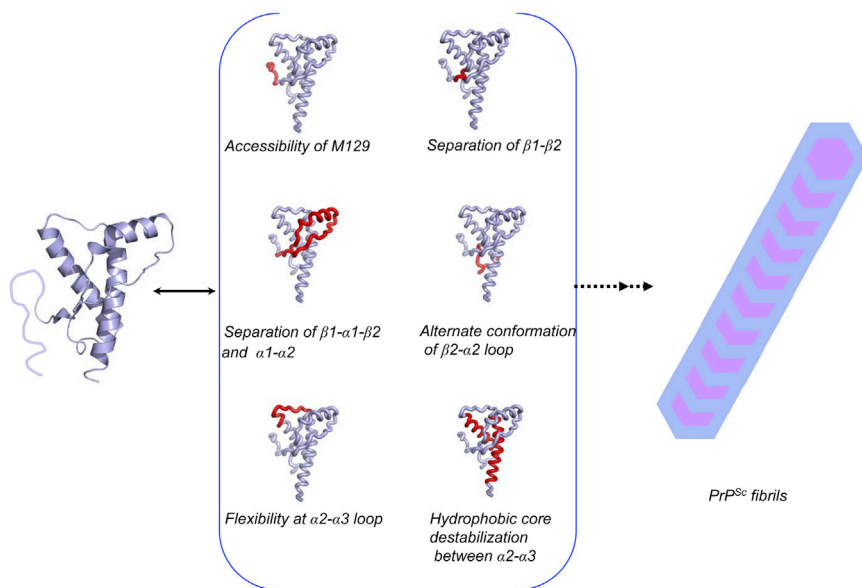


Figure 7. Initiator Motifs in Prion

Several misfolding initiator motifs are observed in the structured domain of prion protein. These include exposure at Met129, separation of $\beta 1$ - $\beta 2$, unfolding of prion subdomains; $\beta 1$ - $\alpha 1$ - $\beta 2$ and $\alpha 2$ - $\alpha 3$, alternate conformation of $\beta 2$ - $\alpha 2$ loop, flexibility at $\alpha 2$ - $\alpha 3$ loop, and hydrophobic core destabilization between $\alpha 2$ - $\alpha 3$. Generation of PrP^{Sc} can be possible due to lethal progression involving individual or multiple toxic motifs. See also Figure S6.

obtained within 7 days. These crystals were soaked briefly for 1–2 min in solution containing 1–10 mM concentrations of phenothiazine derivatives. The selected crystals were then flash frozen in liquid nitrogen after the addition of 20% ethylene glycol as a cryoprotectant.

Data Collection, Structure Determination, and Refinement

Full data sets from the small molecule soaked crystals of the POM1 Fab:moPrP(117–230) complex were collected at beamline 9-2 of the Stanford Synchrotron Radiation Lightsources (SSRL) and at the beamline 19ID at the Advanced Photon Source (APS). The measured data were processed with the HKL2000 suite of programs (Otwinowski and Minor, 1997), and data collection statistics are presented in Table 1. The structure of the complex was solved by the molecular replacement method using the program MOLREP from the CCP4 package (Winn et al., 2011), using the structure of POM1 Fab (PDB ID: 4H88) as a search model. The obtained models of the POM1 Fab:moPrP(117–230) complex were then refined using the Refmac package (Murshudov et al., 2011). After the initial rounds of refinement, clear density for the ligands was visible in the difference electron density maps ($2|F_o| - |F_c|$) and $|F_o| - |F_c|$ electron density maps, and satisfactory hydrogen bond networks with either protein atoms or water molecules were accepted. All of the model building was performed with COOT (Emsley and Cowtan, 2004). The final coordinates of the POM1 Fab:moPrP(117–230) complexes bound with promazine and chlorpromazine have been deposited in the Research Collaboratory for Structural Bioinformatics (RCSB) Protein Data Bank with the PDB ID 4MA7 for the promazine complex and 4MA8 for the chlorpromazine complex. The residue numbering scheme of huPrP was used for moPrP in both the complexes.

Expression and Purification of [U - ^{15}N] shPrP(90–232)

The shPrP90–232 construct cloned into a pET15b expression vector was obtained from PrP5. The plasmid was transformed into BL21-CodonPlus (DE3)-RIL cells (Stratagene) by heat-shock, and an isolated colony was grown overnight in 50 ml of LB broth. This starter culture was inoculated (in a 1:100 ratio) into 1 l of M9 media with 1 g/l of unlabeled NH_4Cl at 37°C with shaking at 200 rpm. The cells were allowed to reach an OD of 0.6, after which they were exchanged into M9 media with 1 g/l of ^{15}N -ammonium sulfate and induced with 1 mM IPTG. The induced culture was allowed to grow for 16–18 hr at 37°C with shaking at 200 rpm. The cells were then harvested by centrifugation at 8,000 rpm for 30 min at 4°C. Further extraction and purification of the protein was performed as described above. The protein was stored in buffer containing 10 mM BIS-TRIS, 100 mM Na_2HPO_4 , pH 5.8.

Production and Purification of POM1 Fab

The POM1 hybridoma was generated as described previously (Polymenidou et al., 2008). In order to purify secreted IgG, the hybridoma supernatant was loaded on to a protein G Sepharose column (PIERCE) and eluted with 0.1 M glycine, pH 2.8. For production of POM1 Fab, 1 mg/ml of POM1 IgG was digested with papain at an IgG:papain ratio of 1:0.02 (w/w) in buffer containing 50 mM TRIS, 150 mM NaCl, 2 mM EDTA, and 2 mM cysteine, pH 8, for 5 hr at 37°C in a water bath. Enzymatic digestion was terminated by addition of 3 mM iodoacetamide. The digest was subsequently concentrated and buffer exchanged with protein A binding buffer (PIERCE) and loaded onto a protein A Sepharose column (Pierce) to remove the F_c fragment and undigested IgG POM1. The purified POM1 Fab fragment was directly collected in the flow-through. The Fab fractions were assessed for homogeneity by Coomassie brilliant blue staining after separation by SDS-PAGE.

Protein Complex Preparation, Crystallization, and Soaking

The POM1 Fab and the purified moPrP (residues 117–230) were mixed in an equimolar ratio and the resulting complex was purified by size exclusion chromatography using a Superdex G-75 column (Amersham Biosciences). The chromatography buffer contained 50 mM TRIS, 100 mM NaCl, and 1 mM NaN_3 , pH 7. For the purposes of crystallization, the purified protein complex was concentrated to 10 mg/ml. High-throughput crystal trays (96-well Intelli-Plates, Hampton Research) were set up by the sitting drop vapor-diffusion method using a robot (Hydra 96 plus one, Robbins Scientific), in which 0.4 μ l of the protein sample was mixed with an equal volume of the screening solution. An initial crystallization hit was found in a saturating solution of 25% PEG3350, 0.1 M MES pH 6.5, and 0.1 M lithium sulfate. After several optimization steps, crystals with approximate dimensions of 0.6 \times 0.1 \times 0.1 mm were

NMR Sample Preparation and Data Recording

All the NMR experiments were acquired at 25°C on a 600 MHz Varian Unity INOVA spectrometer with a 5 mm HCN probe with triple-axis pulsed field gradients and the Varian BioPack Pulse sequence library. All spectra acquired were processed using NMRPIPE (Delaglio et al., 1995) and analyzed with CARRA (Keller, 2004) and SPARKY (Goddard and Kneller, University of California, San Francisco; <http://www.cgl.ucsf.edu/home/sparky>). The 2D ^{15}N -HSQC NMR experiments were acquired using 1,126 complex points over a spectral width of 8,800.88 Hz in the direct dimension (1H) and 128 complex points over a spectral width of 1,882 Hz in the indirect dimension (^{15}N). Sixteen transients were collected for all 2D experiments using a recycle delay of 1.5 s. 2,2-dimethyl-2-silapentane-5-sulfonate (DSS) was used for chemical shift referencing. For titration experiments with promazine, a reference 2D ^{15}N -HSQC spectrum was collected using 500 μ M shPrP(90–232) in buffer containing 9:1 $H_2O:D_2O$, 20 mM KH_2PO_4 , pH 6.2. Subsequently, 2D ^{15}N -HSQC

NMR spectra were acquired by addition of promazine to concentrations of 0.5, 1, 6, and 12 mM. Chemical shifts were assigned according to those in deposition Biological Magnetic Resonance Data Bank (BMRB) 17834.

MD Simulations

MD simulations were conducted for 20 ns using the Sander module and the *ff12SB* force field in the AMBER 12 package (Salomon-Ferrer et al., 2013). The starting structural model for moPrP(119–225) bound to promazine was taken from the crystal structure of POM1 Fab:moPrP:promazine (PDB ID: 4MA7). For the unbound moPrP(119–225) starting structure, promazine molecule was removed. Force field parameters for the promazine molecule were generated using *am1bcc* semi-empirical quantum mechanical methods, as implemented in the program *antechamber* (Wang et al., 2006). The bound and free moPrP(119–225) proteins were placed in a rectangular box filled with TIP3P water molecules. The rectangular box was placed at a distance of 10 Å from the protein surface. One sodium ion was placed in the vicinity of the negatively charged residue at the protein surface in order to neutralize the system. Prior to MD simulation, the protein geometry was optimized in two stages with different constraints. In the first stage (1,500 steps), only water molecules were relaxed, while the protein and the ligand molecule were constrained using a harmonic potential with a force constant of 20 kcal/(mol Å²). For the second minimization stage (2,500 steps), no constraints were employed; protein and solvent were minimized together. The above geometry-optimized system consisting of 17,661 atoms was simulated using periodic boundary conditions. The particle-mesh Ewald method (Darden et al., 1993) was used to calculate the electrostatics interactions with a nonbonded interaction cut-off of 12 Å. During the first part of the equilibration (100 ps of heating from 0 to 310 K), the *NVT* ensemble was used, while all the subsequent simulations were carried out at constant temperature and pressure (310 K and 1 atm, *NPT* ensemble). Bond lengths involving hydrogen were constrained with the SHAKE algorithm (Lippert et al., 2007), and the time step for all MD simulation was set to 2 fs.

ACCESSION NUMBERS

The Protein Data Bank accession numbers for the coordinates and structure factors reported in this paper are 4MA7 and 4MA8.

SUPPLEMENTAL INFORMATION

Supplemental Information includes six figures and can be found with this article online at <http://dx.doi.org/10.1016/j.str.2013.11.009>.

ACKNOWLEDGMENTS

This work has been funded by PrioNet Canada and APRI/ALMA through grants to M.N.G. J. L.S. thanks the Canadian Institutes of Health Research (CIHR) and Alberta Innovates-Health Solutions for financial support. X-ray diffraction data were collected at the Stanford Synchrotron Radiation Lightsource (SSRL) and the Advanced Photon Source (APS). The simulations described here were performed in Westgrid/Compute Canada facilities. The PrioNet Prion Protein and Plasmid Production Facility, University of Alberta provided the prion clones (moPrP full length, shPrP 90-232).

Received: September 3, 2013

Revised: November 19, 2013

Accepted: November 20, 2013

Published: December 26, 2013

REFERENCES

Agrimi, U., Nonno, R., Dell'Omo, G., Di Bari, M.A., Conte, M., Chiappini, B., Esposito, E., Di Guardo, G., Windl, O., Vaccari, G., and Lipp, H.P. (2008). Prion protein amino acid determinants of differential susceptibility and molecular feature of prion strains in mice and voles. *PLoS Pathog.* 4, e1000113.

Aguzzi, A., and Polymenidou, M. (2004). Mammalian prion biology: one century of evolving concepts. *Cell* 116, 313–327.

Antonyuk, S.V., Trevitt, C.R., Strange, R.W., Jackson, G.S., Sangar, D., Batchelor, M., Cooper, S., Fraser, C., Jones, S., Georgiou, T., et al. (2009). Crystal structure of human prion protein bound to a therapeutic antibody. *Proc. Natl. Acad. Sci. USA* 106, 2554–2558.

Apetri, A.C., Surewicz, K., and Surewicz, W.K. (2004). The effect of disease-associated mutations on the folding pathway of human prion protein. *J. Biol. Chem.* 279, 18008–18014.

Baral, P.K., Wieland, B., Swayampakula, M., Polymenidou, M., Rahman, M.H., Kav, N.N., Aguzzi, A., and James, M.N. (2012). Structural studies on the folded domain of the human prion protein bound to the Fab fragment of the antibody POM1. *Acta Crystallogr. D Biol. Crystallogr.* 68, 1501–1512.

Bertsch, U., Winklhofer, K.F., Hirschberger, T., Bieschke, J., Weber, P., Hartl, F.U., Tavan, P., Tatzelt, J., Kretzschmar, H.A., and Giese, A. (2005). Systematic identification of antiprion drugs by high-throughput screening based on scanning for intensely fluorescent targets. *J. Virol.* 79, 7785–7791.

Bradford, M.M. (1976). A rapid and sensitive method for the quantitation of microgram quantities of protein utilizing the principle of protein-dye binding. *Anal. Biochem.* 72, 248–254.

Brundin, P., Melki, R., and Kopito, R. (2010). Prion-like transmission of protein aggregates in neurodegenerative diseases. *Nat. Rev. Mol. Cell Biol.* 11, 301–307.

Castilla, J., Saá, P., Hetz, C., and Soto, C. (2005). In vitro generation of infectious scrapie prions. *Cell* 121, 195–206.

Caughey, B., Baron, G.S., Chesebro, B., and Jeffrey, M. (2009). Getting a grip on prions: oligomers, amyloids, and pathological membrane interactions. *Annu. Rev. Biochem.* 78, 177–204.

Chakraborty, N., Fornili, A., Prigent, S., Kleinjung, J., Dreiss, C.A., Rezaei, H., and Fraternali, F. (2013). Decrypting Prion Protein Conversion into a β -Rich Conformer by Molecular Dynamics. *J. Chem. Theory Comput.* 9, 2455–2465.

Christen, B., Damberger, F.F., Pérez, D.R., Hornemann, S., and Wüthrich, K. (2013). Structural plasticity of the cellular prion protein and implications in health and disease. *Proc. Natl. Acad. Sci. USA* 110, 8549–8554.

Collinge, J. (2001). Prion diseases of humans and animals: their causes and molecular basis. *Annu. Rev. Neurosci.* 24, 519–550.

Collinge, J., Sidle, K.C., Meads, J., Ironside, J., and Hill, A.F. (1996). Molecular analysis of prion strain variation and the aetiology of 'new variant' CJD. *Nature* 383, 685–690.

Collinge, J., Gorham, M., Hudson, F., Kennedy, A., Keogh, G., Pal, S., Rossor, M., Rudge, P., Siddique, D., Spyer, M., et al. (2009). Safety and efficacy of quinacrine in human prion disease (PRION-1 study): a patient-preference trial. *Lancet Neurol.* 8, 334–344.

Corsaro, A., Thellung, S., Bucciarelli, T., Scotti, L., Chiovitti, K., Villa, V., D'Arrigo, C., Aceto, A., and Florio, T. (2011). High hydrophobic amino acid exposure is responsible of the neurotoxic effects induced by E200K or D202N disease-related mutations of the human prion protein. *Int. J. Biochem. Cell Biol.* 43, 372–382.

Cronier, S., Beringue, V., Bellon, A., Peyrin, J.M., and Laude, H. (2007). Prion strain- and species-dependent effects of antiprion molecules in primary neuronal cultures. *J. Virol.* 81, 13794–13800.

Damberger, F.F., Christen, B., Pérez, D.R., Hornemann, S., and Wüthrich, K. (2011). Cellular prion protein conformation and function. *Proc. Natl. Acad. Sci. USA* 108, 17308–17313.

Darden, T., York, D., and Pedersen, L. (1993). Particle mesh Ewald: an $N \log(N)$ method for Ewald sums in large systems. *J. Chem. Phys.* 98, 10089–10092.

Delaglio, F., Grzesiek, S., Vuister, G.W., Zhu, G., Pfeifer, J., and Bax, A. (1995). NMRPipe: a multidimensional spectral processing system based on UNIX pipes. *J. Biomol. NMR* 6, 277–293.

Doh-Ura, K., Iwaki, T., and Caughey, B. (2000). Lysosomotropic agents and cysteine protease inhibitors inhibit scrapie-associated prion protein accumulation. *J. Virol.* 74, 4894–4897.

- Emsley, P., and Cowtan, K. (2004). Coot: model-building tools for molecular graphics. *Acta Crystallogr. D Biol. Crystallogr.* *60*, 2126–2132.
- Ettaiche, M., Pichot, R., Vincent, J.P., and Chabry, J. (2000). In vivo cytotoxicity of the prion protein fragment 106–126. *J. Biol. Chem.* *275*, 36487–36490.
- Forloni, G., Angeretti, N., Chiesa, R., Monzani, E., Salmona, M., Bugiani, O., and Tagliavini, F. (1993). Neurotoxicity of a prion protein fragment. *Nature* *362*, 543–546.
- Geschwind, M.D., Kuo, A.L., Wong, K.S., Haman, A., Devereux, G., Raudabaugh, B.J., Johnson, D.Y., Torres-Chae, C.C., Finley, R., Garcia, P., et al. (2013). Quinacrine treatment trial for sporadic Creutzfeldt-Jakob disease. *Neurology* *81*, 2015–2023.
- Ghaemmaghami, S., Ahn, M., Lessard, P., Giles, K., Legname, G., DeArmond, S.J., and Prusiner, S.B. (2009). Continuous quinacrine treatment results in the formation of drug-resistant prions. *PLoS Pathog.* *5*, e1000673.
- Goodman, L.S., and Gilman, A. (1970). *The Pharmacological Basis of Therapeutics; a Textbook of Pharmacology, Toxicology, and Therapeutics for Physician and Medical Students, Fourth Edition.* (New York: Macmillan).
- Hafner-Bratkovic, I., Bester, R., Pristovsek, P., Gaedtke, L., Veranic, P., Gaspersic, J., Mancek-Keber, M., Avbelj, M., Polymenidou, M., Julius, C., et al. (2011). Globular domain of the prion protein needs to be unlocked by domain swapping to support prion protein conversion. *J. Biol. Chem.* *286*, 12149–12156.
- Heinemann, U., Krasnianski, A., Meissner, B., Varges, D., Kallenberg, K., Schulz-Schaeffer, W.J., Steinhoff, B.J., Grasbon-Frodol, E.M., Kretzschmar, H.A., and Zerr, I. (2007). Creutzfeldt-Jakob disease in Germany: a prospective 12-year surveillance. *Brain* *130*, 1350–1359.
- Hosszu, L.L., Jackson, G.S., Trevitt, C.R., Jones, S., Batchelor, M., Bhelt, D., Prodromidou, K., Clarke, A.R., Waltho, J.P., and Collinge, J. (2004). The residue 129 polymorphism in human prion protein does not confer susceptibility to Creutzfeldt-Jakob disease by altering the structure or global stability of PrPC. *J. Biol. Chem.* *279*, 28515–28521.
- Jobling, M.F., Stewart, L.R., White, A.R., McLean, C., Friedhuber, A., Maher, F., Beyreuther, K., Masters, C.L., Barrow, C.J., Collins, S.J., and Cappai, R. (1999). The hydrophobic core sequence modulates the neurotoxic and secondary structure properties of the prion peptide 106–126. *J. Neurochem.* *73*, 1557–1565.
- Julien, O., Chatterjee, S., Thiessen, A., Graether, S.P., and Sykes, B.D. (2009). Differential stability of the bovine prion protein upon urea unfolding. *Protein Sci.* *18*, 2172–2182.
- Keller, R.L.J. (2004). *Computer Aided Resonance Assignment Tutorial, First Edition.* (Goldau, Switzerland: Cantina Verlag).
- Kocisko, D.A., Baron, G.S., Rubenstein, R., Chen, J., Kuizon, S., and Caughey, B. (2003). New inhibitors of scrapie-associated prion protein formation in a library of 2000 drugs and natural products. *J. Virol.* *77*, 10288–10294.
- Korth, C., May, B.C., Cohen, F.E., and Prusiner, S.B. (2001). Acridine and phenothiazine derivatives as pharmacotherapeutics for prion disease. *Proc. Natl. Acad. Sci. USA* *98*, 9836–9841.
- Kuwata, K., Nishida, N., Matsumoto, T., Kamatari, Y.O., Hosokawa-Muto, J., Kodama, K., Nakamura, H.K., Kimura, K., Kawasaki, M., Takakura, Y., et al. (2007). Hot spots in prion protein for pathogenic conversion. *Proc. Natl. Acad. Sci. USA* *104*, 11921–11926.
- Lee, S.W., Mou, Y., Lin, S.Y., Chou, F.C., Tseng, W.H., Chen, C.H., Lu, C.Y., Yu, S.S., and Chan, J.C. (2008). Steric zipper of the amyloid fibrils formed by residues 109–122 of the Syrian hamster prion protein. *J. Mol. Biol.* *378*, 1142–1154.
- Lee, S., Antony, L., Hartmann, R., Knaus, K.J., Surewicz, K., Surewicz, W.K., and Yee, V.C. (2010). Conformational diversity in prion protein variants influences intermolecular beta-sheet formation. *EMBO J.* *29*, 251–262.
- Lewis, P.A., Tattum, M.H., Jones, S., Bhelt, D., Batchelor, M., Clarke, A.R., Collinge, J., and Jackson, G.S. (2006). Codon 129 polymorphism of the human prion protein influences the kinetics of amyloid formation. *J. Gen. Virol.* *87*, 2443–2449.
- Lippert, R.A., Bowers, K.J., Dror, R.O., Eastwood, M.P., Gregersen, B.A., Klepeis, J.L., Kolossvary, I., and Shaw, D.E. (2007). A common, avoidable source of error in molecular dynamics integrators. *J. Chem. Phys.* *126*, 046101.
- Meli, M., Gasset, M., and Colombo, G. (2011). Dynamic diagnosis of familial prion diseases supports the $\beta 2$ - $\alpha 2$ loop as a universal interference target. *PLoS ONE* *6*, e19093.
- Murshudov, G.N., Skubák, P., Lebedev, A.A., Pannu, N.S., Steiner, R.A., Nicholls, R.A., Winn, M.D., Long, F., and Vagin, A.A. (2011). REFMAC5 for the refinement of macromolecular crystal structures. *Acta Crystallogr. D Biol. Crystallogr.* *67*, 355–367.
- Nakajima, M., Yamada, T., Kusuvara, T., Furukawa, H., Takahashi, M., Yamauchi, A., and Kataoka, Y. (2004). Results of quinacrine administration to patients with Creutzfeldt-Jakob disease. *Dement. Geriatr. Cogn. Disord.* *17*, 158–163.
- Otwinowski, Z., and Minor, W. (1997). Processing of x-ray diffraction data collected in oscillation mode. *Methods Enzymol.* *276*, 307–326.
- Paramithiotis, E., Pinard, M., Lawton, T., LaBoissiere, S., Leathers, V.L., Zou, W.Q., Estey, L.A., Lamontagne, J., Lehto, M.T., Kondziejewski, L.H., et al. (2003). A prion protein epitope selective for the pathologically misfolded conformation. *Nat. Med.* *9*, 893–899.
- Polymenidou, M., Moos, R., Scott, M., Sigurdson, C., Shi, Y.Z., Yajima, B., Hafner-Bratkovic, I., Jerala, R., Hornemann, S., Wuthrich, K., et al. (2008). The POM monoclonals: a comprehensive set of antibodies to non-overlapping prion protein epitopes. *PLoS ONE* *3*, e3872.
- Prusiner, S.B. (2001). Shattuck lecture—neurodegenerative diseases and prions. *N. Engl. J. Med.* *344*, 1516–1526.
- Richardson, E.P., Jr., and Masters, C.L. (1995). The nosology of Creutzfeldt-Jakob disease and conditions related to the accumulation of PrPCJD in the nervous system. *Brain Pathol.* *5*, 33–41.
- Salmona, M., Malesani, P., De Gioia, L., Gorla, S., Bruschi, M., Molinari, A., Della Vedova, F., Pedrotti, B., Marrari, M.A., Awan, T., et al. (1999). Molecular determinants of the physicochemical properties of a critical prion protein region comprising residues 106–126. *Biochem. J.* *342*, 207–214.
- Salomon-Ferrer, R., Case, D.A., and Walker, R.C. (2013). An overview of the Amber biomolecular simulation package. *Wiley Interdiscip. Rev. Comput. Mol. Sci.* *3*, 198–210.
- Sawaya, M.R., Sambashivan, S., Nelson, R., Ivanova, M.I., Sievers, S.A., Apostol, M.I., Thompson, M.J., Balbirnie, M., Wiltzius, J.J., McFarlane, H.T., et al. (2007). Atomic structures of amyloid cross-beta spines reveal varied steric zippers. *Nature* *447*, 453–457.
- Selvaggini, C., De Gioia, L., Cantù, L., Ghibaudi, E., Diomedea, L., Passerini, F., Forloni, G., Bugiani, O., Tagliavini, F., and Salmona, M. (1993). Molecular characteristics of a protease-resistant, amyloidogenic and neurotoxic peptide homologous to residues 106–126 of the prion protein. *Biochem. Biophys. Res. Commun.* *194*, 1380–1386.
- Sigurdson, C.J., Nilsson, K.P., Hornemann, S., Heikenwalder, M., Manco, G., Schwarz, P., Ott, D., Rüllicke, T., Liberski, P.P., Julius, C., et al. (2009). De novo generation of a transmissible spongiform encephalopathy by mouse transgenesis. *Proc. Natl. Acad. Sci. USA* *106*, 304–309.
- Sigurdson, C.J., Joshi-Barr, S., Bett, C., Winson, O., Manco, G., Schwarz, P., Rüllicke, T., Nilsson, K.P., Margalith, I., Raeber, A., et al. (2011). Spongiform encephalopathy in transgenic mice expressing a point mutation in the $\beta 2$ - $\alpha 2$ loop of the prion protein. *J. Neurosci.* *31*, 13840–13847.
- Solassol, J., Crozet, C., and Lehmann, S. (2003). Prion propagation in cultured cells. *Br. Med. Bull.* *66*, 87–97.
- van der Kamp, M.W., and Daggett, V. (2010). Pathogenic mutations in the hydrophobic core of the human prion protein can promote structural instability and misfolding. *J. Mol. Biol.* *404*, 732–748.
- Wadsworth, J.D., Asante, E.A., Desbruslais, M., Linehan, J.M., Joiner, S., Gowland, I., Welch, J., Stone, L., Lloyd, S.E., Hill, A.F., et al. (2004). Human

prion protein with valine 129 prevents expression of variant CJD phenotype. *Science* 306, 1793–1796.

Walsh, P., Simonetti, K., and Sharpe, S. (2009). Core structure of amyloid fibrils formed by residues 106–126 of the human prion protein. *Structure* 17, 417–426.

Wang, J.M., Wang, W., Kollman, P.A., and Case, D.A. (2006). Automatic atom type and bond type perception in molecular mechanical calculations. *J. Mol. Graph. Model.* 25, 247–260.

Will, R.G. (1999). Prion related disorders. *J. R. Coll. Physicians Lond.* 33, 311–315.

Winn, M.D., Ballard, C.C., Cowtan, K.D., Dodson, E.J., Emsley, P., Evans, P.R., Keegan, R.M., Krissinel, E.B., Leslie, A.G.W., McCoy, A., et al. (2011). Overview of the CCP4 suite and current developments. *Acta Crystallogr. D Biol. Crystallogr.* 67, 235–242.

Yin, S.M., Zheng, Y., and Tien, P. (2003). On-column purification and refolding of recombinant bovine prion protein: using its octarepeat sequences as a natural affinity tag. *Protein Expr. Purif.* 32, 104–109.